



1 **Technical note: on LA-ICP-MS U-Pb dating of unetched and etched apatites**

2 Fanis Abdullin et al.: LA-ICP-MS U-Pb dating of apatites

3 Fanis Abdullin<sup>1</sup>, Luigi Solari<sup>2</sup>, Jesús Solé<sup>3</sup>, Carlos Ortega-Obregón<sup>2</sup>

4 <sup>1</sup>CONACyT-Centro de Geociencias, Campus Juriquilla, UNAM, Querétaro, 76230, Mexico

5 <sup>2</sup>Centro de Geociencias, Campus Juriquilla, UNAM, Querétaro, 76230, Mexico

6 <sup>3</sup>LANGEM, Instituto de Geología, UNAM, Ciudad Universitaria, CDMX, 04510, Mexico

7 **Correspondence:** Fanis Abdullin ([fanis@geociencias.unam.mx](mailto:fanis@geociencias.unam.mx))

8

9 **Abstract**

10 The same unetched and chemically etched apatites from five rock samples were dated with U-Pb  
11 using laser ablation inductively coupled plasma mass spectrometry. The objective of this study is  
12 to demonstrate whether or not the etching, needed for the apatite fission track analysis, impact on  
13 the obtaining of apatite U-Pb ages. The results of this experiment indicate that the etching has no  
14 effect on the determination of apatite U-Pb ages by the laser ablation inductively coupled plasma  
15 mass spectrometry technique. Thus, laser ablation inductively coupled plasma mass spectrometry  
16 may be used safely for simultaneous apatite fission track *in-situ* and U-Pb double dating.

17

18 **Short summary**

19 Unetched and etched apatites of five samples were dated by U-Pb with laser ablation inductively  
20 coupled plasma mass spectrometry. Our experiment demonstrates that the etching, needed for the  
21 apatite fission track dating, has no important effect on the obtaining of U-Pb ages; and therefore,  
22 the laser ablation-based technique can be used for apatite fission track and U-Pb double dating.

23



24 **1 Introduction**

25

26 Apatite,  $\text{Ca}_5(\text{PO}_4)_3[\text{F},\text{Cl},\text{OH}]$ , is the most common phosphate mineral in the Earth's crust and can  
27 be found in practically all igneous and metamorphic rocks, as well as in many ancient and recent  
28 sediments and in certain mineral deposits (Piccoli and Candela, 2002; Morton and Yaxley, 2007;  
29 Webster and Piccoli, 2015). This accessory mineral is often used as a natural thermochronometer  
30 (i.e., for fission track, helium and U–Pb dating; e.g., Zeitler et al., 1987; Wolf et al., 1996; Ehlers  
31 and Farley, 2003; Hasebe et al., 2004; Donelick et al., 2005; Chew and Donelick, 2012; Chew et  
32 al., 2014; Cochrane et al., 2014; Liu et al., 2014; Spikings et al., 2015; Glorie et al., 2017).

33 Presently, apatite fission track (AFT) ages may be obtained rapidly by using LA–ICP–MS  
34 (laser ablation inductively coupled plasma mass spectrometry) for direct measurement of “parent  
35 nuclides”, i.e.,  $^{238}\text{U}$  levels (Cox et al., 2000; Svojtka and Košler, 2002; Hasebe et al., 2004, 2009;  
36 Donelick et al., 2005; Vermeesch, 2017). In addition, the LA–ICP–MS-based technique allows to  
37 date apatites simultaneously by AFT and U–Pb (e.g., Chew and Donelick, 2012; Liu et al., 2014;  
38 Glorie et al., 2017; Bonilla et al., 2020; Nieto-Samaniego et al., 2020). After chemical etching of  
39 apatites, a smaller volume of ablated material is analyzed with LA–ICP–MS. Therefore, there is a  
40 doubt on the application of such double dating technique. The question is how chemical etching,  
41 required for the AFT dating, may influence on the obtaining of apatite U–Pb ages? To respond to  
42 this question, the same unetched and etched apatite crystals from five experimental samples were  
43 dated by LA–ICP–MS U–Pb. The chosen rock samples have either emplacement or metamorphic  
44 ages varying from the Early Cretaceous to the Neoproterozoic (for details, please see Table 1).

45

--- Table 1 ---

46



47 **2 Brief description of samples**

48

49 2.1 OV-0421 (Tres Sabanas Pluton, Guatemala)

50

51 This sample is a two mica-bearing deformed granite belonging to the Tres Sabanas Pluton, which  
52 is located NW of Guatemala City, Guatemala. For sample OV-0421, an emplacement age of 115  
53  $\pm 4$  Ma was proposed based on zircon U–Pb data (Torres de León, 2016). A cooling age of 102  $\pm$   
54 1 Ma, obtained with K–Ar (on biotite concentrate), has also been reported by the same author.

55

56 2.2. MCH-38 (Chiapas Massif Complex, Mexico)

57

58 MCH-38 is an orthogneiss from the Permian Chiapas Massif Complex. This rock was sampled to  
59 the west of Unión Agrarista, the State of Chiapas, southeastern Mexico. There is no reported age  
60 for this sample. Some zircon U–Pb dates obtained for the Chiapas Massif Complex (Weber et al.,  
61 2007, 2008; Ortega-Obregón et al., 2019) suggest that a Lopingian (260–252 Ma) crystallization  
62 or metamorphic age may be assumed for sample MCH-38.

63

64 2.3 TO-AM (Totoltepec Pluton, Mexico)

65

66 TO-AM is a granitic rock, sampled ca. 5 km west of Totoltepec de Guerrero, the State of Puebla,  
67 southern Mexico. There is no reported radiometric data for sample TO-AM. Previous geological  
68 studies indicate that the Pennsylvanian–Cisuralian Totoltepec Pluton was emplaced over a ca. 20  
69 million year period (from 306  $\pm 2$  to 287  $\pm 2$  Ma; e.g., Kirsch et al., 2013).



70

71 2.4 CH-0403 (Altos Cuchumatanes, Guatemala)

72

73 CH-0403 was collected 5 km ESE of Barillas, in the Altos Cuchumatanes, Guatemala. It consists  
74 of a gray to green granodiorite. Five zircon aliquots of sample CH-0403 were dated using isotope  
75 dilution thermal ionization mass spectrometry, yielding a lower intercept date of  $391 \pm 8$  Ma that  
76 is interpreted as its approximate crystallization age (Solari et al., 2009).

77

78 2.5 OC-1008 (Oaxacan Complex, Mexico)

79

80 This sample is a paragneiss from the Grenvillian Oaxacan Complex, southern Mexico. OC-1008  
81 was collected in the federal road which connects Nochixtlán to Oaxaca. It was demonstrated that  
82 this sample underwent “dry” granulite facies metamorphism at  $990 \pm 10$  Ma (Solari et al., 2014).

83

84

### 85 3 Analytical procedures

86

87 Apatites were concentrated using conventional mineral separation techniques. Nearly 300 apatite  
88 grains, extracted from each rock sample, were mounted with EpoFix™ in a 2.5 cm diameter ring.  
89 Apatites were mounted with their surfaces parallel to the crystallographic *c*-axis. Mounted grains  
90 were polished to expose their internal surfaces (i.e., up to  $4\pi$  geometry). For our experiment, only  
91 “sterile” and complete crystals, without visible inclusions and other defects such as cracks, were



92 gently selected. Sample preparation was performed at Taller de Molienda, Centro de Geociencias  
93 (CGEO), Campus Juriquilla, Universidad Nacional Autónoma de Mexico (UNAM).

94 Single spot analyses were performed with a Resonetics RESolution™ LPX Pro (193 nm,  
95 ArF excimer) laser ablation system, coupled to a Thermo Scientific iCAP™ Qc quadrupole ICP-  
96 MS at Laboratorio de Estudios Isotópicos (LEI), CGEO, UNAM. During this experimental work,  
97 LA-ICP-MS-based sampling was performed exactly in central parts of the selected apatite grains  
98 before and after chemical etching (in 5.5M HNO<sub>3</sub> at 21 °C for 20 s to reveal spontaneous fission  
99 tracks), as shown schematically in Fig. 1. The LA-ICP-MS protocol used for apatite analyses, as  
100 given in Table 2, was established on the basis of numerous experiments carried out at LEI during  
101 the past five years, and can be used for U-Pb and fission track double dating plus multielemental  
102 analysis (Abdullin et al., 2018; Ortega-Obregón et al., 2019). Corrected isotopic ratios and errors  
103 were calculated using Iolite (Paton et al., 2011) and the VizualAge data reduction scheme (Petrus  
104 and Kamber, 2012). UcomPbine (Chew et al., 2014) was used to model <sup>207</sup>Pb/<sup>206</sup>Pb initial values  
105 and thus force a <sup>207</sup>Pb correction that considers the common Pb (non-radiogenic Pb) incorporated  
106 by apatite standards at the moment of their crystallization (see also Ortega-Obregón et al., 2019).  
107 The “First Mine Discovery” apatite from Madagascar, with a mean <sup>206</sup>U-<sup>238</sup>Pb age of ca. 480 Ma  
108 (Thomson et al., 2012; Chew et al., 2014), was used as a main reference material. The results for  
109 measured isotopes using the NIST-612 glass (Pearce et al., 1997) were normalized using <sup>43</sup>Ca as  
110 an internal standard and taking an average CaO content of 55% (i.e., for F-apatites).

111 --- **Figure 1** ---

112 --- **Table 2** ---

113

114



## 115 4 Results

116

117 Tera and Wasserburg Concordia diagrams (T–W; Tera and Wasserburg, 1972) are used in apatite  
118 U–Pb dating, because the LA–ICP–MS-derived U–Pb results are generally discordant. The lower  
119 intercept in the T–W plot is considered as a “mean” apatite U–Pb age that should have geological  
120 significance (crystallization or cooling age, or the ages of mineralization or metamorphic event).  
121 Apatite U–Pb ages were calculated with IsoplotR (Vermeesch, 2017, 2018) and described below.  
122 Detailed information on our U–Pb experiments is given in Table S1 in the Supplement.

123

### 124 4.1 OV-0421

125

126 For sample OV-0421, 41 unetched apatites analysed yielded a lower intercept age of  $106 \pm 4$  Ma  
127 with a mean square weighted deviation (MSWD) of 1.07, passing the chi-squared probability test  
128 with the  $P(\chi^2)$  value of 0.35 (see Fig. 2). Virtually the same U–Pb age,  $107 \pm 5$  Ma, was obtained  
129 after chemical etching of the same apatite crystals, yielding a MSWD of 1.13 and a  $P(\chi^2)$  of 0.27.  
130 Both these apatite U–Pb ages lie between the zircon U–Pb age of  $115 \pm 4$  Ma (i.e., crystallization  
131 age) and the biotite K–Ar date of  $102 \pm 1$  Ma (i.e., cooling age), which were previously obtained  
132 for the same granite sample by Torres de León (2016).

133

### 134 4.2. MCH-38

135

136 For orthogneiss sample MCH-38, the lower intercept in T–W yielded a U–Pb age of  $245 \pm 6$  Ma  
137 (obtained from 41 unetched grains) with a MSWD of 0.28 and a  $P(\chi^2)$  of 1. Etched apatite grains



138 from MCH-38 yielded an age of  $240 \pm 4$  Ma with a MSWD of 0.36 and a  $P(\chi^2)$  of 1 (Fig. 2). Our  
139 U–Pb ages are in close agreement with geochronological data reported from the Permian Chiapas  
140 Massif Complex in previous studies (Damon et al., 1981; Torres et al., 1999; Schaaf et al., 2002;  
141 Ortega-Obregón et al., 2019). For instance, Torres et al. (1999) compiled biotite K–Ar ages, most  
142 of which lie within the Early–Middle Triassic period. Triassic cooling ages in the Chiapas Massif  
143 Complex were also detected by Rb–Sr in mica–whole rock pairs that range from  $244 \pm 12$  to  $214$   
144  $\pm 11$  Ma (Schaaf et al., 2002).

145

#### 146 4.3 TO-AM

147

148 Unetched apatites (32 crystals; Fig. 2) from granite TO-AM yielded a lower intercept date of  $303$   
149  $\pm 5$  Ma with a MSWD of 0.6 and a  $P(\chi^2)$  of 0.96. After etching, a slightly younger age of  $299 \pm 3$   
150 Ma was obtained, with a MSWD of 0.89 and a  $P(\chi^2)$  of 0.65. These apatite U–Pb dates are in line  
151 with the zircon U–Pb ages of  $306 \pm 2$  to  $287 \pm 2$  Ma reported for the Pennsylvanian to Cisuralian  
152 Totoltepec Pluton (e.g., see details in Kirsch et al., 2013).

153

#### 154 4.4 CH-0403

155

156 36 unetched apatite grains from sample CH-0403 yielded a lower intercept U–Pb age of  $345 \pm 10$   
157 Ma with a MSWD of 0.7 and a  $P(\chi^2)$  of 0.9, whereas etched grains yielded an age of  $334 \pm 8$  Ma  
158 with a MSWD of 1.37 and a  $P(\chi^2)$  of 0.08 (Fig. 2). These cooling dates are considerably younger  
159 if compared to the CH-0403 emplacement age of  $391 \pm 8$  Ma (Solari et al., 2009).

160



161 4.5 OC-1008

162

163 41 unetched apatites of OC-1008 yielded a U–Pb age of  $839 \pm 12$  Ma with a MSWD of 0.98 and  
164 a  $P(\chi^2)$  of 0.50. After etching, the same apatites yielded an age of  $830 \pm 10$  Ma with a MSWD of  
165 1.24 and a  $P(\chi^2)$  of 0.14 (Fig. 2). Both these apatite U–Pb ages are significantly younger than the  
166 age of granulite facies metamorphism in the Grenville-aged Oaxacan Complex (1 Ga to 980 Ma,  
167 Solari et al., 2014), and thus, can be considered as cooling ages.

168 --- **Figure 2** ---

169

170

## 171 **5 Discussion and concluding remarks**

172

173 Most samples, except OV-0421, yielded slightly younger apatite U–Pb dates after etching (up to  
174 3.3% in sample CH-0403). The lower intercept U–Pb ages obtained from unetched apatite grains  
175 are identical within errors to the U–Pb ages obtained on the same apatites etched (see diagram in  
176 Fig. 3). The results of our experimental study demonstrate that the chemical etching, required for  
177 the AFT analysis, has no important effect on the determination of apatite U–Pb ages by LA–ICP–  
178 MS. Thus, as a conclusion of this work, LA–ICP–MS can be used safely to obtain simultaneously  
179 AFT and U–Pb ages (i.e., double dating), as it was already done in some studies without previous  
180 proof (Chew and Donelick, 2012; Liu et al., 2014; Glorie et al., 2017; Bonilla et al., 2020; Nieto-  
181 Samaniego et al., 2020).

182 --- **Figure 3** ---

183



184

185 **Supplement**

186 The supplement related to this article is available online at: <https://...>

187

188

189 **Author contributions**

190 Conceptualisation, investigation, and writing of the original draft were done by FA. LS and COO

191 provided technical support. LS and JS acquired funding and resources, supervised the study, and

192 reviewed the manuscript.

193

194 **Competing interests**

195 The authors declare that they have no conflict of interest.

196

197

198 **Acknowledgements**

199 The authors are very grateful to Juan Tomás Vázquez Ramírez and Ofelia Pérez Arvizu for their

200 help with sample preparation for this study. Professor Stuart Thomson (University of Arizona) is

201 acknowledged for sharing the Madagascar apatite. Michelangelo Martini kindly provided granite

202 sample TO-AM that was very useful for our experimental study.

203

204 **Financial support**

205 This research has been supported by PAPIIT DGAPA UNAM (grant no. IN101520 to LS).

206



207

208

209 **Figure caption**

210

211

212 **Figure 1**

213 Illustration displaying the LA-ICP-MS-based U-Pb dating of the same apatite crystal before and  
214 after chemical etching (i.e., etched in 5.5M nitric acid at 21 °C for 20 s). Spot diameter of 60 µm.

215

216

217 **Figure 2**

218 Tera-Wasserburg Concordia diagrams for the U-Pb results of unetched and etched apatites from  
219 samples OV-0421, MCH-38, TO-AM, CH-0403, and OC-1008. MSWD – mean square weighted  
220 deviation, Ngr – number of grains dated.

221

222

223 **Figure 3**

224 Binary plot showing the lower intercept U-Pb ages obtained on unetched and etched apatites.

225

226

227

228

229



230

231 **References**

232

233 Abdullin, F., Solari, L., Ortega-Obregón, C., and Solé, J.: New fission-track results from the  
234 northern Chiapas Massif area, SE Mexico: trying to reconstruct its complex thermo-tectonic  
235 history, *Revista Mexicana de Ciencias Geológicas*, 35, 79–92,  
236 <https://doi.org/10.22201/cgeo.20072902e.2018.1.523>, 2018.

237

238 Bonilla, A., Franco, J. A., Cramer, T., Poujol, M., Cogné, N., Nachtergaele, S., and De Grave, J.:  
239 Apatite LA-ICP-MS U–Pb and fission-track geochronology of the Caño Viejita gabbro in E-  
240 Colombia: Evidence for Grenvillian intraplate rifting and Jurassic exhumation in the NW  
241 Amazonian Craton, *Journal of South American Earth Sciences*, 98, 102438,  
242 <https://doi.org/10.1016/j.jsames.2019.102438>, 2020.

243

244 Chew, D. M., and Donelick, R. A.: Combined apatite fission track and U-Pb dating by LA-ICP-  
245 MS and its application in apatite provenance analysis, *Quantitative Mineralogy and*  
246 *Microanalysis of Sediments and Sedimentary Rocks: Mineralogical Association of Canada,*  
247 *Short Course*, 42, 219–247, 2012.

248

249 Chew, D. M., Petrus, J. A., and Kamber, B. S.: U–Pb LA–ICPMS dating using accessory mineral  
250 standards with variable common Pb, *Chemical Geology*, 363, 185–199,  
251 <https://doi.org/10.1016/j.chemgeo.2013.11.006>, 2014.

252



253

254 Cochrane, R., Spikings, R. A., Chew, D., Wotzlaw, J. F., Chiaradia, M., Tyrrell, S., Schaltegger,  
255 U., and Van der Lelij, R.: High temperature ( $> 350$  °C) thermochronology and mechanisms of Pb  
256 loss in apatite, *Geochimica et Cosmochimica Acta*, 127, 39–56,  
257 <https://doi.org/10.1016/j.gca.2013.11.028>, 2014.

258

259 Cox, R., Košler, J., Sylvester, P., and Hodych, P.: Apatite fission-track (FT) dating by LAM-  
260 ICP-MS analysis, Goldschmidt Conference, Oxford, UK, *Journal of Conference Abstracts*, 5, p.  
261 322, 2000.

262

263 Damon, P. E., Shafiqullah, M., and Clark, K. F.: Age trends of igneous activity in relation to  
264 metallogenesis in the southern Cordillera, Tucson, Arizona, *Arizona Geological Society Digest*,  
265 14, 137–153, 1981.

266

267 Donelick, R. A., O’Sullivan, P. B., and Ketcham, R. A.: Apatite fission-track analysis, *Reviews*  
268 *in Mineralogy and Geochemistry*, 58, 49–94, <https://doi.org/10.2138/rmg.2005.58.3>, 2005.

269

270 Ehlers, T. A., and Farley, K. A.: Apatite (U–Th)/He thermochronometry: methods and  
271 applications to problems in tectonic and surface processes, *Earth and Planetary Science Letters*,  
272 206, 1–14, [https://doi.org/10.1016/S0012-821X\(02\)01069-5](https://doi.org/10.1016/S0012-821X(02)01069-5), 2003.

273

274

275



- 276 Glorie, S., Alexandrov, I., Nixon, A., Jepson, G., Gillespie, J., and Jahn, B. M.: Thermal and  
277 exhumation history of Sakhalin Island (Russia) constrained by apatite U-Pb and fission track  
278 thermochronology, *Journal of Asian Earth Sciences*, 143, 326–342,  
279 <https://doi.org/10.1016/j.jseaes.2017.05.011>, 2017.  
280
- 281 Hasebe, N., Barbarand, J., Jarvis, K., Carter, A., and Hurford, A. J.: Apatite fission-track  
282 chronometry using laser ablation ICP-MS, *Chemical Geology*, 207, 135–145,  
283 <https://doi.org/10.1016/j.chemgeo.2004.01.007>, 2004.  
284
- 285 Hasebe, N., Carter, A., Hurford, A. J., and Arai, S.: The effect of chemical etching on LA-ICP-  
286 MS analysis in determining uranium concentration for fission-track chronometry, *Geological*  
287 *Society, London, Special Publications*, 324, 37–46, <https://doi.org/10.1144/SP324.3>, 2009.  
288
- 289 Kirsch, M., Keppie, J. D., Murphy, J. B., and Lee, J. K.: Arc plutonism in a transtensional  
290 regime: the late Palaeozoic Totoltepec pluton, Acatlán Complex, southern Mexico, *International*  
291 *Geology Review*, 55, 263–286, <https://doi.org/10.1080/00206814.2012.693247>, 2013.  
292
- 293 Liu, W., Zhang, J., Sun, T., Wang, J.: Application of apatite U-Pb and fission-track double  
294 dating to determine the preservation potential of magnetite-apatite deposits in the Luzong and  
295 Ningwu volcanic basins, eastern China, *Journal of Geochemical Exploration*, 138, 22–32,  
296 <https://doi.org/10.1016/j.gexplo.2013.12.006>, 2014.  
297  
298



299 Morton, A., and Yaxley, G.: Detrital apatite geochemistry and its application in provenance  
300 studies, *Special Papers, Geological Society of America*, 420, 319,  
301 [https://doi.org/10.1130/2006.2420\(19\)](https://doi.org/10.1130/2006.2420(19)), 2007.  
302  
303 Nieto-Samaniego, A. F., Olmos-Moya, M. D. J. P., Levresse, G., Alaniz-Alvarez, S. A.,  
304 Abdullin, F., del Pilar-Martínez, A., and Xu, S.: Thermochronology and exhumation rates of  
305 granitic intrusions at Mesa Central, Mexico, *International Geology Review*, 62, 311–319,  
306 <https://doi.org/10.1080/00206814.2019.1602789>, 2020.  
307  
308 Ortega-Obregón, C., Abdullin, F., Solari, L., Schaaf, P., and Solís-Pichardo, G.: Apatite U-Pb  
309 dating at UNAM laboratories: analytical protocols and examples of its application, *Revista*  
310 *Mexicana de Ciencias Geológicas*, 36, 27–37,  
311 <https://doi.org/10.22201/cgeo.20072902e.2019.1.749>, 2019.  
312  
313 Paton, C., Hellstrom, J., Paul, B., Woodhead, J., Hergt, J.: Iolite: Freeware for the visualisation  
314 and processing of mass spectrometric data, *Journal of Analytical Atomic Spectrometry*, 26,  
315 2508–2518, <https://doi.org/10.1039/C1JA10172B>, 2011.  
316  
317 Pearce, N. J., Perkins, W. T., Westgate, J. A., Gorton, M. P., Jackson, S. E., Neal, C. R., and  
318 Chenery, S. P.: A compilation of new and published major and trace element data for NIST SRM  
319 610 and NIST SRM 612 glass reference materials, *Geostandards newsletter*, 21, 115–144,  
320 <https://doi.org/10.1111/j.1751-908X.1997.tb00538.x>, 1997.  
321



322

323 Petrus, J. A., and Kamber, B. S.: VizualAge: A novel approach to laser ablation ICP-MS U-Pb  
324 geochronology data reduction, *Geostandards and Geoanalytical Research*, 36, 247–270,  
325 <https://doi.org/10.1111/j.1751-908X.2012.00158.x>, 2012.

326

327 Piccoli, P. M., and Candela, P. A.: Apatite in igneous systems, *Reviews in Mineralogy and*  
328 *Geochemistry*, 48, 255–292, <https://doi.org/10.2138/rmg.2002.48.6>, 2002.

329

330 Schaaf, P., Weber, B., Weis, P., Groß, A., Ortega-Gutiérrez, F., and Kohler, H.: The Chiapas  
331 Massif (Mexico) revised: New geologic and isotopic data and basement characteristics, *Neues*  
332 *Jahrbuch für Geologie und Paläontologie, Abhandlungen*, 225, 1–23, 2002.

333

334 Solari, L. A., Ortega-Gutiérrez, F., Elías-Herrera, M., Schaaf, P., Norman, M., Ortega-Obregón,  
335 C., and Chiquín, M.: U-Pb zircon geochronology of Palaeozoic units in western and central  
336 Guatemala: Insights into the tectonic evolution of Middle America, *Geological Society, London,*  
337 *Special Publications*, 328, 295–313, <https://doi.org/10.1144/SP328.12>, 2009.

338

339 Solari, L. A., Ortega-Gutiérrez, F., Elías-Herrera, M., Ortega-Obregón, C., Macías-Romo, C.,  
340 Reyes-Salas, M.: Detrital provenance of the Grenvillian Oaxacan Complex, southern Mexico: a  
341 zircon perspective, *International Journal of Earth Sciences*, 103, 1301–1315,  
342 <https://doi.org/10.1007/s00531-013-0938-9>, 2014.

343

344



345 Spikings, R., Cochrane, R., Villagomez, D., Van der Lelij, R., Vallejo, C., Winkler, W., and  
346 Beate, B.: The geological history of northwestern South America: From Pangaea to the early  
347 collision of the Caribbean large igneous province (290–75 Ma), *Gondwana Research*, 27, 95–  
348 139, <https://doi.org/10.1016/j.gr.2014.06.004>, 2015.

349

350 Svojtka, M., and Košler: Fission-track dating of zircon by LA-ICP-MS, Goldschmidt  
351 Conference, Davos, Switzerland, *Journal of Conference Abstracts, Special Supplement of*  
352 *Geochimica et Cosmochimica Acta*, 66, A756, 2002.

353

354 Tera, F., and Wasserburg, G. J.: U-Th-Pb systematics in three Apollo 14 basalts and the problem  
355 of initial Pb in lunar rocks, *Earth and Planetary Science Letters*, 14, 281–304,  
356 [https://doi.org/10.1016/0012-821X\(72\)90128-8](https://doi.org/10.1016/0012-821X(72)90128-8), 1972.

357

358 Thomson, S. N., Gehrels, G. E., Ruiz, J., and Buchwaldt, R.: Routine low-damage apatite U-Pb  
359 dating using laser ablation–multicollector–ICPMS, *Geochemistry, Geophysics, Geosystems*,  
360 13(2), <https://doi.org/10.1029/2011GC003928>, 2012.

361

362 Torres, R., Ruiz, J., Patchett, P. J., Grajales, J. M., Bartolini, C., Wilson, J. L., and Lawton, T. F.:  
363 Permo-Triassic continental arc in eastern Mexico: Tectonic implications for reconstruction of  
364 southern North America, *Geological Society of America, Special Papers*, 340, 191–196,  
365 <https://doi.org/10.1130/0-8137-2340-X.191>, 1999.

366

367



- 368 Torres de León, R.: Caracterización geológica y geocronológica de unidades metamórficas e  
369 intrusivas de la región centro–Oeste de la Cuenca del Río Motagua, Sureste de Guatemala,  
370 Centroamerica: implicaciones en las conexiones Sur de México–Bloque Chortís, Universidad  
371 Nacional Autónoma de México, Posgrado en Ciencias de la Tierra, Ph.D Thesis, 221 pp., 2016.  
372
- 373 Vermeesch, P.: Statistics for LA-ICP-MS based fission track dating, *Chemical Geology*, 456,  
374 19–27, <https://doi.org/10.1016/j.chemgeo.2017.03.002>, 2017.  
375
- 376 Vermeesch, P.: IsoplotR: A free and open toolbox for geochronology, *Geoscience Frontiers*, 9,  
377 1479–1493, <https://doi.org/10.1016/j.gsf.2018.04.001>, 2018.  
378
- 379 Weber, B., Iriondo, A., Premo, W. R., Hecht, L., and Schaaf, P.: New insights into the history  
380 and origin of the southern Maya block, SE Mexico: U–Pb–SHRIMP zircon geochronology from  
381 metamorphic rocks of the Chiapas massif, *International Journal of Earth Sciences*, 96, 253–269,  
382 <https://doi.org/10.1007/s00531-006-0093-7>, 2007.  
383
- 384 Weber, B., Valencia, V. A., Schaaf, P., Pompa-Mera, V., and Ruiz, J.: Significance of  
385 provenance ages from the Chiapas Massif Complex (southeastern Mexico): redefining the  
386 Paleozoic basement of the Maya Block and its evolution in a peri-Gondwanan realm, *The  
387 Journal of Geology*, 116, 619–639, <https://doi.org/10.1086/591994>, 2008.  
388
- 389 Webster, J. D., and Piccoli, P. M.: Magmatic apatite: A powerful, yet deceptive, mineral,  
390 *Elements*, 11, 177–182, <https://doi.org/10.2113/gselements.11.3.177>, 2015.



391

392 Wolf, R. A., Farley, K. A., and Silver, L. T.: Helium diffusion and low-temperature  
393 thermochronometry of apatite, *Geochimica et Cosmochimica Acta*, 60, 4231–4240,  
394 [https://doi.org/10.1016/S0016-7037\(96\)00192-5](https://doi.org/10.1016/S0016-7037(96)00192-5), 1996.

395

396 Zeitler, P. K., Herczeg, A. L., McDougall, I., and Honda, M.: U-Th-He dating of apatite: A  
397 potential thermochronometer, *Geochimica et Cosmochimica Acta*, 51, 2865–2868,  
398 [https://doi.org/10.1016/0016-7037\(87\)90164-5](https://doi.org/10.1016/0016-7037(87)90164-5), 1987.

399

400

401

402

403

404

405

406

407

408

409

410

411

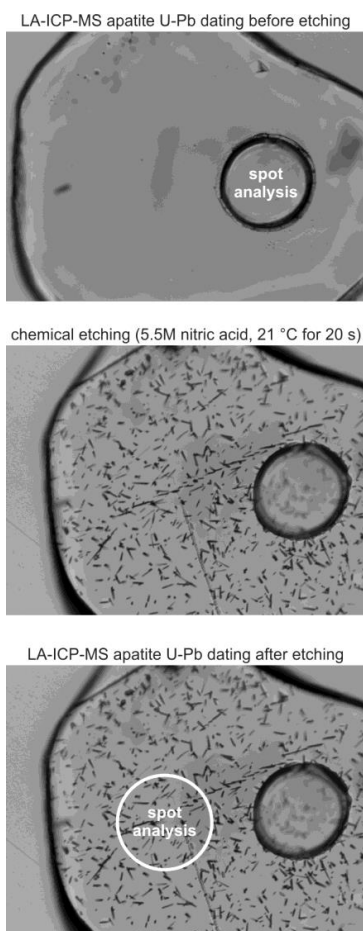
412

413



414

**Figure 1**



415

416

417

418

419

420

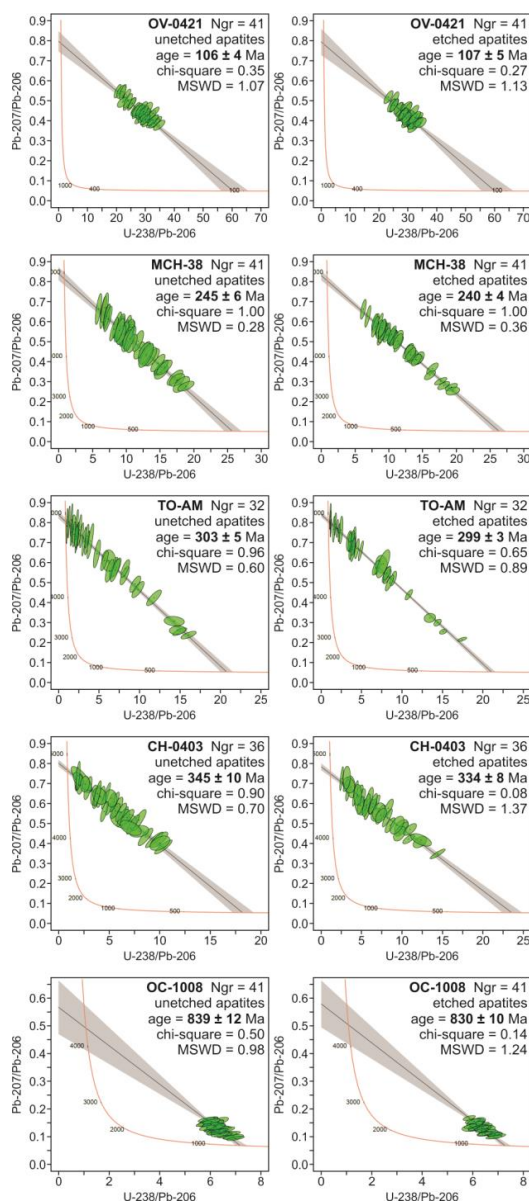
421

422



423

Figure 2



424

425

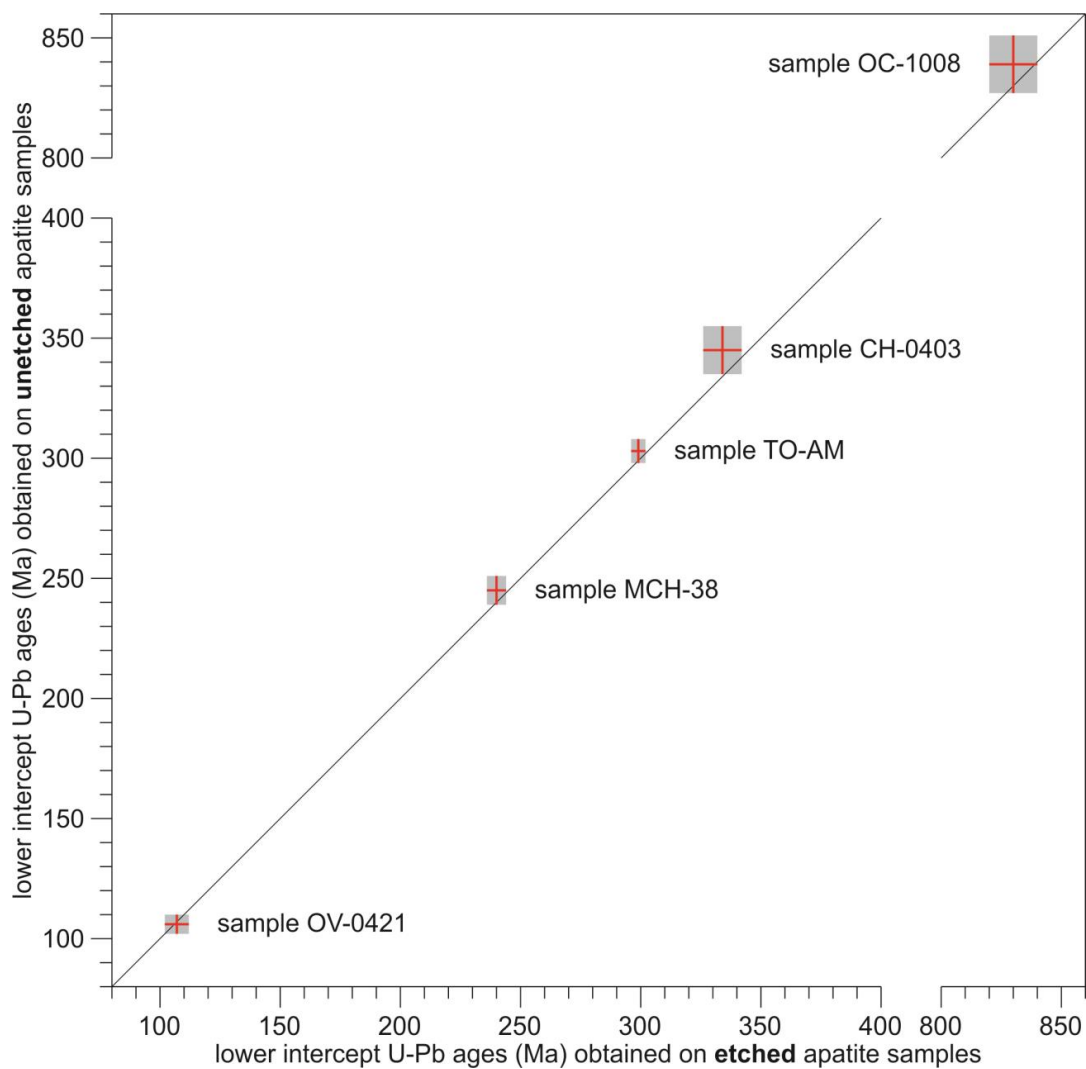
426

427



428

Figure 3



429

430

431

432

433

434



435

436 **Table 1**

437

438 Lithology, locality, and zircon U–Pb data for the selected experimental rock samples.

Sample	Unit and locality	Rock type	Zircon U–Pb age	References
OV-0421	Tres Sabanas Pluton, Guatemala	deformed granite	115 ± 4 Ma	Torres de León (2016)
MCH-38	Chiapas Massif Complex, Mexico	orthogneiss	ca. 260 to ca. 252 Ma (?)	Weber et al. (2007, 2008)
TO-AM	Totoltepec Pluton, Mexico	granite	ca. 308 to ca. 285 Ma (?)	Kirsch et al. (2013)
CH-0403	Altos Cuchumatanes, Guatemala	granodiorite	391 ± 8 Ma	Solari et al. (2009)
OC-1008	Oaxacan Complex, Mexico	paragneiss	990 ± 10 Ma	Solari et al. (2014)

439

440

441

442

443

444

445

446

447

448

449

450

451

452

453



454

455 **Table 2**

456

457 LA–ICP–MS protocol established at LEI to be applied for simultaneous apatite U–Pb and fission-  
 458 track *in-situ* double dating plus multielemental analysis (REEs, Y, Sr, Mn, Mg, Th, U, and Cl).

<i>ICP-MS operating conditions</i>	
Instrument	Thermo Scientific™ iCAP™ Qc
Forward power	1450 W
Carrier gas flow rate	~1 L/min (Ar) and ~0.35 L/min (He)
Auxiliary gas flow rate	~1 L/min
Plasma gas flow rate	~14 L/min
Nitrogen	~3.5 mL/min
<i>Data acquisition parameters</i>	
Mode of operating	STD (standard mode)
Sampling scheme	–2NIST-612–2MAD–1DUR–10apts–
Background scanning	15 s
Data acquisition time	35 s
Wash-out time	15 s
Measured isotopes	<sup>43</sup> Ca <sup>44</sup> Ca <sup>31</sup> P <sup>35</sup> Cl <sup>26</sup> Mg <sup>55</sup> Mn <sup>88</sup> Sr <sup>89</sup> Y <sup>139</sup> La <sup>140</sup> Ce <sup>141</sup> Pr <sup>146</sup> Nd <sup>147</sup> Sm <sup>153</sup> Eu <sup>157</sup> Gd <sup>159</sup> Tb <sup>163</sup> Dy <sup>165</sup> Ho <sup>166</sup> Er <sup>169</sup> Tm <sup>172</sup> Yb <sup>175</sup> Lu <sup>232</sup> Th <sup>238</sup> U <sup>204</sup> Pb <sup>206</sup> Pb <sup>207</sup> Pb <sup>208</sup> Pb <sup>202</sup> Hg [total = 29]
<i>Laser ablation system</i>	
Ablation cell	RESOLUTION™ Laurin Technic S-155
Model of laser	Resonetics RESOLUTION™ LPX Pro
Wavelength	193 nm (Excimer ArF)
Repetition rate	4 Hz
Energy density	*4 J/cm <sup>2</sup>
Mode of sampling	spot diameter of 60 μm

459

460 Note: MAD – “First mine Discovery” U–Pb apatite standard from Madagascar; DUR – Durango  
 461 apatite from Cerro de Mercado mine (Mexico); apts – unknown apatites. (\*) Constant laser pulse  
 462 energy of 4 J/cm<sup>2</sup>, which was measured directly on target with a Coherent™ laser energy meter.

463